THE JOURNAL OF PHYSICAL CHEMISTRY A
A JOURNAL OF THE AMERICAN CHEMICAL SOCIETY

pubs.acs.org/JPCA

Article

The 235−360 GHz Rotational Spectrum of 1-Oxaspiro[2.5]octa-4,7-dien-6-one—Analysis of the Ground Vibrational State and Its 10 Lowest-Energy Vibrationally Excited States

Brian J. Esselman, Edward B. Pimentel, William H. Styers, Dairen R. Jean, R. Claude Woods,* and Robert J. McMahon*

Cite This: *J. Phys. Chem. A* 2024, 128, 191−203

Read Online

ACCESS | Metrics & More | Article Recommendations | Supporting Information

ABSTRACT: The millimeter-wave rotational spectrum of 1-oxaspiro[2.5]octa-4,7-dien-6-one (**1**) was collected from 235 to 360 GHz. With the rotational spectrum of this compound available for the first time, more than 5500 *a*- and *c*-type transitions were observed and assigned for the vibrational ground state. These transitions were least-squares fit to S- and A-reduced, sextic distorted-rotor Hamiltonians in the I^r representation (σ_{fit} = 37 kHz). Additionally, transitions of four fundamental states (ν_{22}, ν_{21}, ν_{39}, and ν_{38}), four overtone states ($2\nu_{22}$, $3\nu_{22}$, $4\nu_{22}$, and $5\nu_{22}$), and two combination states ($\nu_{22} + \nu_{21}$ and $\nu_{22} + \nu_{39}$) were measured, assigned, and least-squares fit to single-state, S- and A-reduced, sextic distorted-rotor Hamiltonians in the I^r representation (σ_{fit} < 42 kHz). The computed vibration−rotation interaction constants ($B_0 - B_v$) (MP2 and B3LYP/6-311+G(2d,p)) were compared to their corresponding experimental values, showing excellent agreement for all fundamental states. Based on the intensities of the transitions from six members of the v ν_{22} series, the fundamental frequency of ν_{22} was determined to be 79.0 (2.1) cm^{-1}.

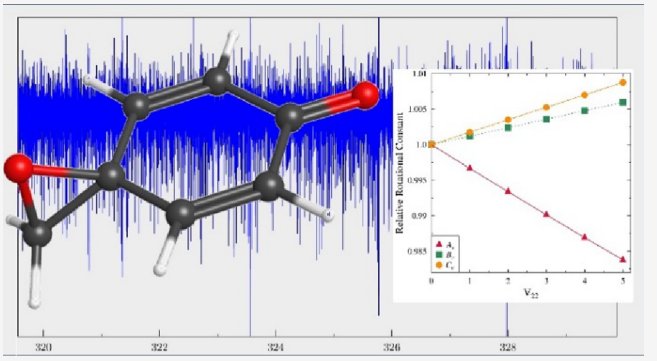

INTRODUCTION

1-Oxaspiro[2.5]octa-4,7-dien-6-one (**1**, Figure 1) presents an interesting structural motif in which a strained epoxide ring shares a carbon atom with a cyclohexadienone ring. Such spirocyclic ring junctions are somewhat uncommon in organic chemistry, and the involvement of a strained ring typically confers high reactivity. Structurally, compound **1** may be considered as the adduct of *p*-benzoquinone and methylene (CH_2) or, alternatively, as the epoxide of 4-methylene-cyclohexadienone (Figure 2). 1-Oxaspiro[2.5]octa-4,7-dien-6-one (**1**) is a nonaromatic, higher-energy isomer of benzoic acid, a molecule previously studied by rotational spectroscopy.[1,2] Despite being a relatively simple molecule that contains only seven carbon atoms, this compound has not received much attention in the literature.[3−9] Compound **1** is a C_s, prolate, asymmetric rotor. The presence of two oxygen atoms in the *ac* plane of the molecule generates a larger *a* axis and a

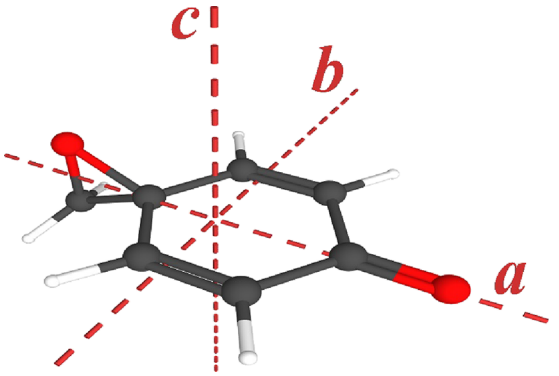

Figure 1. 1-Oxaspiro[2.5]octa-4,7-dien-6-one (**1**, $C_7H_6O_2$, C_s) with principal inertial axes (μ_a = 3.17 D, μ_c = 1.67 D; MP2).

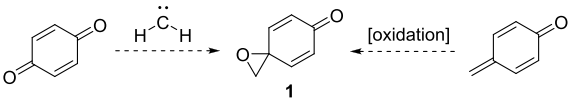

Figure 2. 1-Oxaspiro[2.5]octa-4,7-dien-6-one (**1**): structural relationships to *p*-benzoquinone and 4-methylene-cyclohexadienone.

Received: October 24, 2023
Revised: November 25, 2023
Accepted: November 27, 2023
Published: December 28, 2023

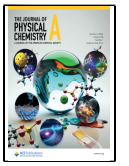

smaller *c*-axis dipole moment component (Figure 1). No previous gas-phase spectroscopy has been reported for this reasonably volatile compound with a substantial dipole moment.

1-Oxaspiro[2.5]octa-4,7-dien-6-one (**1**) was first synthesized by the oxidation of *p*-hydroxybenzyl alcohol using sodium bismuthate.[7,8] Its polymerization[6] and reactivity in Diels–Alder reactions[4,5] have been reported. Recently, McLaughlin et al. reported synthesis of **1** from the bis-dichloroacetate of 4-hydroxybenzyl alcohol using hydrogen peroxide,[3] which was the synthetic route employed in this work. Additionally, they demonstrated that its multiple electrophilic sites can be selectively targeted by judicious choice of a nucleophile.[3] Our spectroscopic study of this compound began somewhat fortuitously when **1** was synthesized to determine whether it was one of several byproducts from the biocatalytic oxidation of phenol derivatives. We were intrigued by its unique structure and the fact that there are very few spirocyclic compounds studied by rotational spectroscopy.[10−15] Three of these compounds, 1-oxaspiro[2.5]octane,[11] 6,6-dimethyl-1-oxaspiro[2.5]octane,[12] and oxaspiro[2.2]pentane,[15] contain epoxide functionalities similar to 1-oxaspiro[2.5]octa-4,7-dien-6-one (**1**).

EXPERIMENTAL AND COMPUTATIONAL METHODS

Synthesis. Our synthesis of **1** followed the procedure reported by McLaughlin et al. as shown in Scheme 1.[3] 4-Hydroxybenzyl alcohol (**2**) was converted to the activated bis(dichloroacetate) ester (**3**) using dichloroacetyl chloride. Activated substrate **3** was then converted to 1-oxaspiro[2.5]-octa-4,7-dien-6-one (**1**) via an *in situ*-generated *p*-quinone methide intermediate that is epoxidized using Weitz–Scheffer conditions.[16,17]

Scheme 1. Synthesis of 1-Oxaspiro[2.5]octa-4,7-dien-6-one (1) from 4-Hydroxybenzyl Alcohol (2)

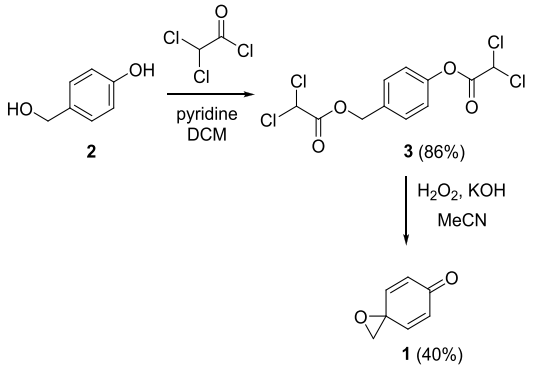

Spectroscopy. The prepared sample was introduced to a millimeter-wave spectrometer that has been previously described.[18,19] The complete spectrum from 235 to 360 GHz was obtained using automated data collection software in less than 2.5 days with these experimental parameters: 0.6 MHz/s sweep rate, 10 ms time constant, and 50 kHz AM and 500 kHz FM modulation in a tone-burst design.[20] The rotational spectra were collected in a continuous flow with a sample pressure of 5 mTorr to maintain a high partial pressure of 1-oxaspiro[2.5]octa-4,7-dien-6-one, despite a low leak rate over the 2.5 days of data collection. The prepared sample showed no observable decomposition during the course of our spectroscopic investigation. Kisiel's Assignment and Analysis of Broadband Spectra (AABS) software was used to analyze the experimental spectrum.[21,22] Pickett's SPFIT/SPCAT[23] was used for least-squares fitting, and analyses were completed using PIFORM, PLANM, and AC.[24,25] An assumed uncertainty of 50 kHz was used for all of the measured frequencies.

Computation. The optimized molecular geometries of **1** and other $C_7H_6O_2$ isomers were obtained using very tight convergence criteria with an ultrafine integration grid (opt = verytight and int = grid = ultrafine) using Gaussian 16 through the WebMO interface.[26,27] Computations were performed at the B3LYP/6-311+G(2d,p) and MP2/6-311+G(2d,p) levels of theory. Predicted values of the fundamental vibrational frequencies, spectroscopic constants, vibration–rotation interaction constants ($B_0 - B_v$), quartic and sextic centrifugal distortion constants, Coriolis coupling constants, and anharmonicity constants were determined by using an anharmonic frequency calculation. Computational output files are provided in the Supporting Information.

RESULTS

1-Oxaspiro[2.5]octa-4,7-dien-6-one (**1**) has not been previously studied by rotational spectroscopy, unlike its $C_7H_6O_2$ isomers benzoic acid,[1,2] phenyl formate,[28] salicylaldehyde,[29] 1,3-benzodioxole,[30] and tropolone.[31] The optimized structures of these $C_7H_6O_2$ isomers, along with the 3-hydroxy and 4-hydroxy isomers of salicylaldehyde, were obtained at the B3LYP/6-311+G(2d,p) level of theory in order to place the relative energy of the oxaspiro isomer **1** in context (Figure 3).

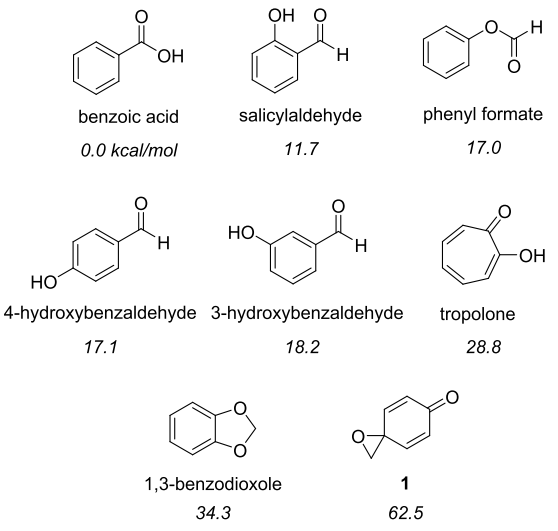

Figure 3. Computed relative energies (kcal/mol; B3LYP/6-311+G(2d,p) including ZPVE) of selected $C_7H_6O_2$ isomers.

The lowest-energy isomer, benzoic acid, is more stable by 62.5 kcal/mol, including ZPVE, than **1**. Each of the aromatic isomers of $C_7H_6O_2$ shown in Figure 3 is substantially more stable than **1**, often by more than 30 kcal/mol due to the loss of aromaticity and the presence of a strained three-membered ring in the latter. To our knowledge, **1** is the highest-energy and only nonaromatic $C_7H_6O_2$ isomer studied by rotational spectroscopy.

https://doi.org/10.1021/acs.jpca.3c07049
J. Phys. Chem. A 2024, 128, 191−203

Ground Vibrational State. Without experimental spectroscopic constants from a previous work, the initial prediction and assignment were accomplished using computed spectroscopic constants and dipole moments at both the B3LYP and MP2 levels of theory with the 6-311+G(2d,p) basis set. These values proved sufficiently accurate to allow assignment and least-squares fitting of the low K_a series. As shown in Figure 4,

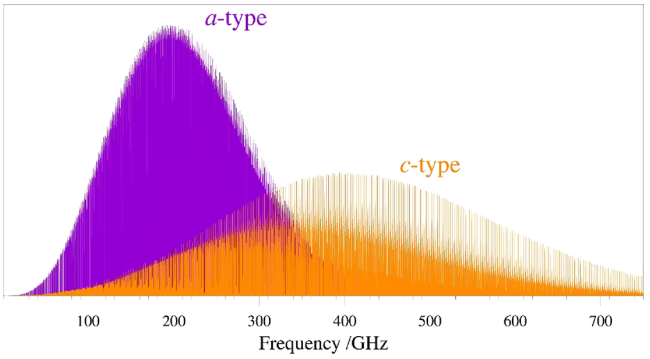

Figure 4. Predicted rotational spectrum of the ground vibrational state of 1-oxaspiro[2.5]octa-4,7-dien-6-one up to 750 GHz at 292 K. *a*-type transitions are displayed in purple, and *c*-type transitions are displayed in orange.

the spectral range measured in this work (235−360 GHz) includes a large number of *a*-type and *c*-type transitions with J'' from 27 to 178 and K_a'' from 0 to 69. Given the need to synthesize a sample and the extensive J/K coverage of the observed transitions, additional spectra at higher or lower frequencies were not collected.

The spectral region from 254 to 257 GHz (Figure 5) showcases the spectral density of the 1-oxaspiro[2.5]octa-4,7-dien-6-one spectrum. The initial fitting of the spectra in our observed frequency region required the use of Loomis−Wood plots to locate the transitions of the K_a = 0 series using computed spectroscopic constants. Having determined adequate values of C_0 and D_J using the K_a = 0 series, assigning transitions to other low-K_a series was straightforward using the Loomis−Wood plots. Throughout this process, it was quite challenging to visually discern a clear pattern of transitions due to the spectral density and lack of clear band structures. Indeed, even with a prediction based upon the final fit shown in Figure 5, there is not an obvious prolate-type R-branch band structure discernible in the experimental spectrum. Due to the size of the molecule and resulting small rotational constants, the spectrum displays a very high line density, with >5000 transitions for the ground state between 235 and 360 GHz. Prominent vibrationally excited states each contribute several thousand additional, intense transitions. There are many thousands of additional unassigned transitions from the vibrationally excited states that are higher in energy than the 11 studied in this work. In fact, the spectral density is so high over the observed frequency range that it is not clear if the spectrum ever shows a clean baseline. As a result of the intrinsic spectral density of each vibrational state and the many vibrational states that display transition intensities that exceed those predicted for the mono-^{13}C isotopologues, no transitions were assigned in this work to any isotopologues.

The final data set includes many *a*-type and *c*-type R-branch transitions ($^aR_{0,1}$ and $^cR_{1,0}$) and *c*-type Q-branch transitions ($^cQ_{1,-2}$ and $^cQ_{1,0}$). The *a*-type R-branch transitions range in J'' from 104 to 179. As expected from the predicted spectrum in Figure 4, the *c*-type R-branch transitions cover a much lower range of J'' values, ranging from 28 to 123. The smaller number of *c*-type Q-branch transitions covers a range of J'' values already available to the data set via the *a*-type R-branch transitions. The final data set, represented in the data distribution plot in Figure 6, includes over 5500 independent transitions. The density of the spectrum, variety of transition

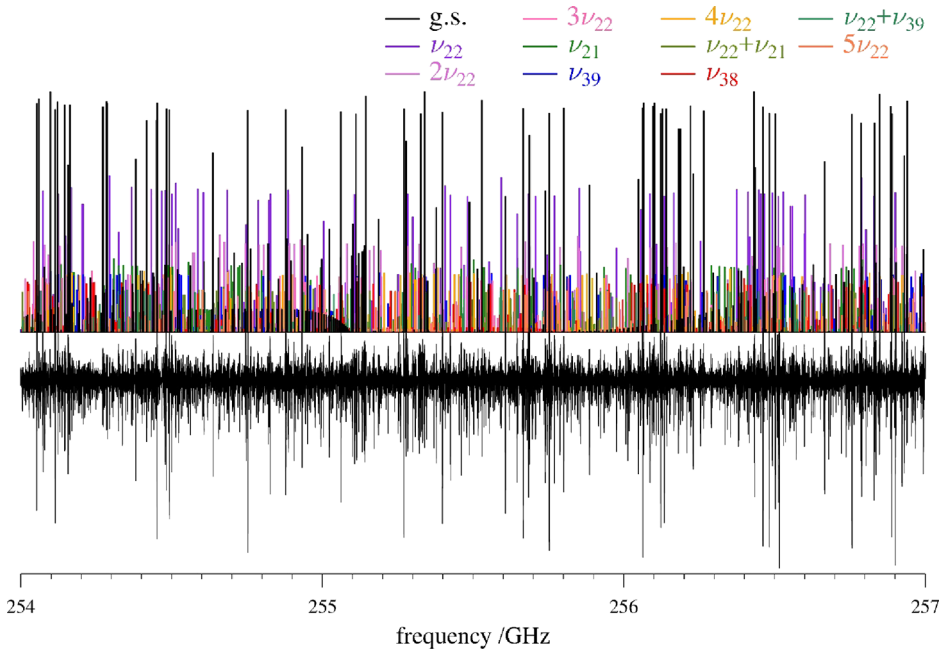

Figure 5. Predicted (top) and experimental (bottom) rotational spectra of 1-oxaspiro[2.5]octa-4,7-dien-6-one from 254 to 257 GHz, showcasing the spectral density and lack of clear, isolated band structures. Unassigned transitions can be attributed to other vibrationally excited states of 1-oxaspiro[2.5]octa-4,7-dien-6-one.

https://doi.org/10.1021/acs.jpca.3c07049
J. Phys. Chem. A 2024, 128, 191−203

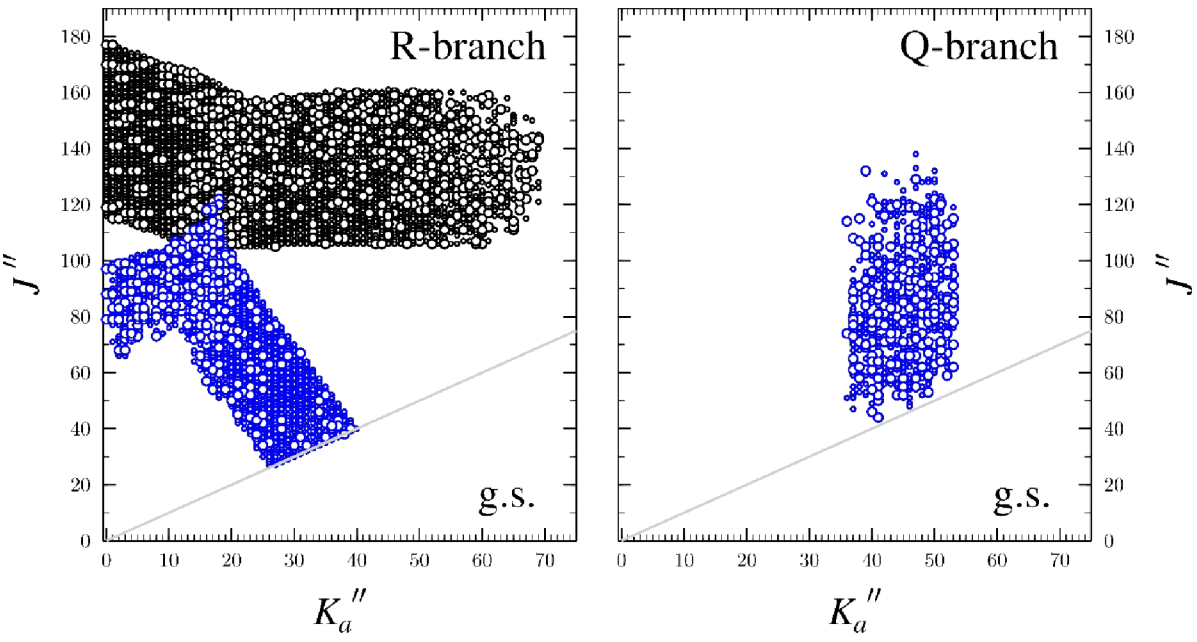

Figure 6. Data distribution plots for the least-squares fit of spectroscopic data for the vibrational ground state of 1-oxaspiro[2.5]octa-4,7-dien-6-one (S reduction, I^r representation), with *a*-type transitions in black and *c*-type transitions in blue. The size of the outlined circles in this plot corresponds to $|(f_{obsd} - f_{calcd})/\delta f|$, where δf is the measurement uncertainty and all quotient values are less than 3.

types, extensive J/K quantum number range, and large number of transitions in the final data set allowed for an excellent determination of a complete sextic distorted-rotor Hamiltonian in both the A and S reductions using the I^r representation. The resulting spectroscopic constants are presented in Table 1, along with their corresponding computed constants at the B3LYP/6-311+G(2d,p) and MP2/6-311+G(2d,p) levels of theory.

The computed rotational constants using both B3LYP and MP2 are in good agreement with the experimental values, with the largest discrepancies being less than 0.8%. Given the very high J'' values for the $K_a = 0$ series of the *a*-type, R-branch transitions, the small deviations in the predicted C_0 constants represent a discrepancy of 2.4 GHz at the top of the frequency range. While these predicted constants were sufficient to identify the $K_a = 0$ series transitions, as mentioned above, care was needed to get the correct J'' assignments of the individual transitions. The computed quartic centrifugal distortion constants are also in reasonable agreement with the experimental values. The B3LYP calculation appears to predict these distortion constants slightly better, but both methods generate quartic distortion constants that are within 15% of the experimental values (δ_K and d_2). The computed sextic centrifugal distortion constants are within 25% of their experimental values. Collectively, the comparison between theory and experiment provides confidence in the computational methods to generate meaningful spectroscopic constants and in the physical meaning of the constants derived from experimental analysis.

Spectral Analysis of ν_{22}. The first fundamental state, ν_{22} (A′, 77 cm^{-1} B3LYP; 69 cm^{-1} MP2) involves large, symmetric motions of the carbonyl oxygen atom and the epoxide group with respect to the six-membered ring, causing a slight ring deformation. Like the ground vibrational state, ν_{22} and all of the vibrationally excited states investigated in this work were adequately treated with single-state, distorted-rotor Hamiltonians. The S reduction and I^r representation spectroscopic constants determined for all vibrationally excited states studied in the current work are presented in Table 2. The corresponding data set distribution plots, as well as the A reduction and I^r constants, can be found in the Supporting Information. Given the low-error fit of the ground-state transitions and the fact that the next fundamental (ν_{21}) is nearly 150 cm^{-1} higher in energy (Figure 7), it is not surprising that over 4100 ν_{22} transitions could be adequately treated with a single-state, distorted-rotor Hamiltonian (σ_{fit} = 36 kHz). As with the ground vibrational state, the data set for ν_{22} is sufficient to determine a complete set of rotational, quartic, and sextic spectroscopic constants. The computed vibration−rotation interaction constants ($B_0 - B_{22}$) of ν_{22} show excellent agreement with their experimentally determined values (Table 3). The largest discrepancy is for the B3LYP value of $B_0 - B_{22}$, where the computed value was underestimated by 90 kHz or 6.4%. The quartic and sextic centrifugal distortion constants show expected small deviations from their corresponding ground-state constants, indicating that these values are likely to be physically meaningful. As will be discussed in detail below, the same conclusion can be drawn from the data presented in Tables 2 and 3 for each of the vibrationally excited states studied in this work. Unless otherwise noted, as with ν_{22}, no evidence of untreated Coriolis or anharmonic coupling was observed in the transition frequencies or the spectroscopic parameters determined for any of the vibrationally excited states. Despite recent advances in the ability to predict the centrifugal distortion constants of 1*H*- and 2*H*-1,2,3-triazole,[32] prediction of the centrifugal distortion constants of ν_{22} and the other vibrationally excited states of 1-oxaspiro[2.5]octa-4,7-dien-6-one (**1**) is nontrivial and well beyond the scope of this work. The spectroscopic constants of ν_{22}, however, can be compared to the corresponding values of other members of the v ν_{22} series to assess their quality (*vide infra*). This analysis provides additional confidence in the physical meaning of the spectroscopic constants for the associated excited states.

https://doi.org/10.1021/acs.jpca.3c07049
J. Phys. Chem. A 2024, 128, 191−203

Table 1. Experimental and Computational Spectroscopic Constants for the Ground Vibrational State of 1-Oxaspiro[2.5]octa-4,7-dien-6-one (S- and A-Reduced Hamiltonians, I^r Representation)

S reduction, I^r representation				A reduction, I^r representation			
	experimental	B3LYP[a]	MP2[a]		experimental	B3LYP[a]	MP2[a]
$A_0^{(S)}$ (MHz)	4419.272694 (92)	4426	4399	$A_0^{(A)}$ (MHz)	4419.272673 (91)	4426	4399s
$B_0^{(S)}$ (MHz)	1198.964182 (35)	1191	1189	$B_0^{(A)}$ (MHz)	1198.964091 (35)	1191	1189
$C_0^{(S)}$ (MHz)	1007.133151 (35)	1001	1000	$C_0^{(A)}$ (MHz)	1007.133242 (35)	1001	1000
D_J (kHz)	0.0303296 (19)	0.0288	0.0297	Δ_J (kHz)	0.0296657 (19)	0.0283	0.0290
D_{JK} (kHz)	0.1329370 (91)	0.128	0.138	Δ_{JK} (kHz)	0.1369164 (90)	0.131	0.142
D_K (kHz)	0.587549 (54)	0.584	0.566	Δ_K (kHz)	0.584224 (54)	0.581	0.563
d_1 (kHz)	−0.00535179 (55)	−0.00508	−0.00522	δ_J (kHz)	0.00535178 (55)	0.00508	0.00522
d_2 (kHz)	0.00033203 (14)	0.000286	0.000350	δ_K (kHz)	−0.045929 (19)	−0.0403	−0.0495
H_J (Hz)	0.000002874 (33)	0.00000258	0.00000314	Φ_J (Hz)	0.000002133 (36)	0.00000198	0.00000232
H_{JK} (Hz)	0.00011479 (18)	0.0000871	0.000113	Φ_{JK} (Hz)	0.0000876 (16)	0.0000661	0.0000884
H_{KJ} (Hz)	−0.0024335 (18)	−0.00194	−0.00246	Φ_{KJ} (Hz)	−0.0023333 (57)	−0.00186	−0.00237
H_K (Hz)	0.0018399 (98)	0.00167	0.00207	Φ_K (Hz)	0.001767 (10)	0.00161	0.00200
h_1 (Hz)	0.000000398 (14)	0.000000421	0.000000412	ϕ_J (Hz)	0.000000343 (15)	0.000000377	0.000000359
h_2 (Hz)	−0.0000003725 (56)	−0.000000303	−0.000000410	ϕ_{JK} (Hz)	−0.00004791 (76)	−0.0000395	−0.0000540
h_3 (Hz)	−0.0000000563 (29)	−0.0000000438	−0.0000000531	ϕ_K (Hz)	−0.000766 (36)	−0.000612	−0.000748
N_{lines}[b]	5561			N_{lines}[b]	5561		
σ_{fit} (MHz)	0.037			σ_{fit} (MHz)	0.037		
κ[c]	−0.888	−0.889	−0.889	κ[c]	−0.888	−0.889	−0.889
Δ_i (μÅ^2)[d]	−34.071379 (21)	−33.6	−34.3	Δ_i (μÅ^2)[d]	−34.071457 (21)	−33.6	−34.3

[a]Calculation using the 6-311+G(2d,p) basis set. Values converted to the right-handed coordinate system from the left-handed coordinate system in the Gaussian output file. [b]Number of independent transition frequencies. [c]$\kappa = (2B - A - C)/(A - C)$, calculated using PLANM. [d]Inertial defect ($\Delta_i = I_c - I_a - I_b$) calculated from the B_0 constants using PLANM.

https://doi.org/10.1021/acs.jpca.3c07049
J. Phys. Chem. A 2024, 128, 191−203

Table 2. Spectroscopic Constants for 1-Oxaspiro[2.5]octa-4,7-dien-6-one in Its Ground State and Low-Energy, Vibrationally Excited States (S-Reduced Hamiltonian, I^r Representation)

	ground state	ν_{22} (A′, 77 cm^{-1})[a]	$2\nu_{22}$ (A′, 154 cm^{-1})[a]	ν_{21} (A′, 223 cm^{-1})[a]	$3\nu_{22}$ (A′, 230 cm^{-1})[a]
$A_v^{(S)}$ (MHz)	4419.272694 (92)	4404.53106 (12)	4389.99632 (16)	4408.01674 (27)	4375.66216 (17)
$B_v^{(S)}$ (MHz)	1198.964182 (35)	1200.393859 (45)	1201.824198 (49)	1200.467935 (76)	1203.254545 (68)
$C_v^{(S)}$ (MHz)	1007.133151 (35)	1008.895015 (43)	1010.657452 (61)	1008.231552 (69)	1012.420643 (80)
D_J (kHz)	0.0303296 (19)	0.0310877 (24)	0.0318554 (28)	0.0306650 (39)	0.0326223 (37)
D_{JK} (kHz)	0.1329370 (91)	0.122939 (14)	0.113209 (18)	0.133737 (23)	0.103698 (27)
D_K (kHz)	0.587549 (54)	0.594875 (70)	0.60163 (10)	0.56390 (26)	0.607661 (68)
d_1 (kHz)	−0.00535179 (55)	−0.00534138 (69)	−0.00533289 (26)	−0.0053709 (11)	−0.00532043 (31)
d_2 (kHz)	0.00033203 (14)	0.00033747 (19)	0.00034234 (13)	0.00032107 (36)	0.00034849 (15)
H_J (Hz)	0.000002874 (33)	0.000003504 (43)	0.000004191 (48)	0.000003099 (71)	0.000004809 (63)
H_{JK} (Hz)	0.00011479 (18)	0.00009790 (31)	0.00008321 (42)	0.00010237 (64)	0.00006893 (72)
H_{KJ} (Hz)	−0.0024335 (18)	−0.0021485 (35)	−0.0019125 (54)	−0.0022704 (80)	−0.001691 (11)
H_K (Hz)	0.0018399 (98)	0.001569 (13)	0.001335 (22)	0.001893 (88)	[0.0011379]
h_1 (Hz)	0.000000398 (14)	0.000000470 (18)	[0.000000541][b]	0.000000496 (29)	[0.000000613][b]
h_2 (Hz)	−0.0000003725 (56)	−0.0000003868 (72)	[−0.000000401][b]	−0.000000400 (13)	[−0.000000415][b]
h_3 (Hz)	−0.0000000563 (29)	−0.0000000577 (33)	[−0.0000000591][b]	−0.0000000480 (52)	[−0.0000000605][b]
N_{lines}[c]	5561	4146	3066	2513	2118
σ_{fit} (MHz)	0.037	0.036	0.038	0.040	0.040
κ[d]	−0.888	−0.887	−0.887	−0.887	−0.887
Δ_i (μÅ^2)[e]	−34.071379 (21)	−34.828410 (27)	−35.580776 (35)	−34.382068 (44)	−36.328891 (46)

	ν_{39} (A″, 265 cm^{-1})[a]	$\nu_{22}+\nu_{21}$ (A′, 301 cm^{-1})[a]	$4\nu_{22}$ (A′, 304 cm^{-1})[a]	ν_{38} (A″, 318 cm^{-1})[a]	$\nu_{22}+\nu_{39}$ (A″, 342 cm^{-1})[a]	$5\nu_{22}$ (A′, 378 cm^{-1})[a]
$A_v^{(S)}$ (MHz)	4417.22303 (50)	4393.40451 (83)	4361.52580 (33)	4428.38462 (94)	4402.53496 (29)	4347.58001 (24)
$B_v^{(S)}$ (MHz)	1198.981090 (92)	1201.89418 (14)	1204.685219 (97)	1198.93050 (17)	1200.41449 (60)	1206.11500 (22)
$C_v^{(S)}$ (MHz)	1007.42665 (11)	1009.98189 (16)	1014.18443 (12)	1006.66034 (20)	1009.181344 (86)	1015.949353 (59)
D_J (kHz)	0.0304077 (48)	0.0313809 (68)	0.0333884 (52)	0.0302761 (89)	0.0311395 (45)	0.0341819 (12)
D_{JK} (kHz)	0.129601 (42)	0.12403 (11)	0.094492 (66)	0.12882 (13)	0.120022 (67)	0.085189 (46)
D_K (kHz)	0.59228 (46)	0.56803 (67)	0.61399 (15)	0.61077 (73)	0.59762 (13)	0.620008 (91)
d_1 (kHz)	−0.00538695 (78)	−0.0053428 (16)	−0.00530477 (78)	−0.0053514 (20)	−0.0053694 (35)	[−0.00529]
d_2 (kHz)	0.00035318 (79)	0.00032118 (50)	0.00035479 (33)	0.00029774 (58)	0.0003593 (11)	[0.000357]
H_J (Hz)	0.000002774 (85)	0.00000304 (12)	0.000005454 (91)	0.00000465 (16)	[0.00000340]	[0.00000644]
H_{JK} (Hz)	0.0001103 (11)	0.0000400 (30)	0.0000527 (15)	0.0001235 (45)	[0.0000934]	[0.0000316]
H_{KJ} (Hz)	−0.002388 (19)	−0.002175 (66)	−0.001502 (41)	−0.002645 (73)	[−0.00210]	[−0.00142]
H_K (Hz)	0.00156 (14)	0.00144 (17)	[0.0009777]	0.00116 (18)	[0.00129]	[0.000854]
h_1 (Hz)	[0.000000398]	[0.000000568]	[0.000000684]	[0.000000398]	[0.000000398]	[0.000000758]
h_2 (Hz)	−0.000000259 (24)	[−0.000000414]	[−0.000000430]	[−0.000000372]	[−0.000000273]	[−0.000000444]
h_3 (Hz)	−0.0000000571 (76)	[−0.0000000494]	[−0.0000000619]	[−0.0000000563]	[−0.0000000585]	[−0.0000000633]
N_{lines}[c]	1690	969	1117	753	500	506
σ_{fit} (MHz)	0.042	0.040	0.041	0.042	0.038	0.042
κ[c]	−0.888	−0.887	−0.886	−0.888	−0.887	−0.886
Δ_i (μÅ^2)[d]	−34.264691 (65)	−35.132511 (96)	−37.072567 (69)	−33.61223 (12)	−35.01532 (22)	−37.81268 (82)

[a]Anharmonic frequencies calculated at the B3LYP/6-311+G(2d,p) level. Overtones $3\nu_{22}$, $4\nu_{22}$, and $5\nu_{22}$ estimated from the anharmonicity constant.[33] [b]Bracketed values held constant at their respective ground-state value or a value extrapolated from lower-energy vibrational states using an appropriate polynomial. [c]Number of independent transition frequencies. [d]$\kappa = (2B - A - C)/(A - C)$, using PLANM. [e]Inertial defect ($\Delta_i = I_c - I_a - I_b$) calculated from the B_v constants using PLANM.

Spectral Analysis of $2\nu_{22}$. The next lowest-energy vibrationally excited state is the first overtone, $2\nu_{22}$ (A′, 154 cm^{-1} B3LYP; 137 cm^{-1} MP2), which can be treated as a distorted rotor, despite being only about 50 cm^{-1} lower than the next vibrational mode, ν_{21}. The spectroscopic constants of $2\nu_{22}$ are very well predicted by linear extrapolation from the vibrational ground state and ν_{22}. With over 3000 transitions, a partial set of sextic centrifugal distortion constants was determined with a low-error (σ_{fit} = 38 kHz) least-squares fit (Table 2). The analysis of the entire series of v ν_{22} spectroscopic constants later revealed that the off-diagonal sextic constants (h_1, h_2, and h_3) were not consistent with those determined for the ground vibrational state and ν_{22}. Thus, the spectroscopic constants presented in Table 2 have values for those three parameters held constant at their linearly extrapolated values. As a result, we are confident that the remaining spectroscopic constants are not substantially impacted by the off-diagonal sextic constants not being allowed to vary in the least-squares fit.

Spectral Analysis of ν_{21}. The second fundamental, ν_{21} (A′, 223 cm^{-1} B3LYP; 210 cm^{-1} MP2), is similar to ν_{22}, except that

https://doi.org/10.1021/acs.jpca.3c07049
J. Phys. Chem. A 2024, 128, 191−203

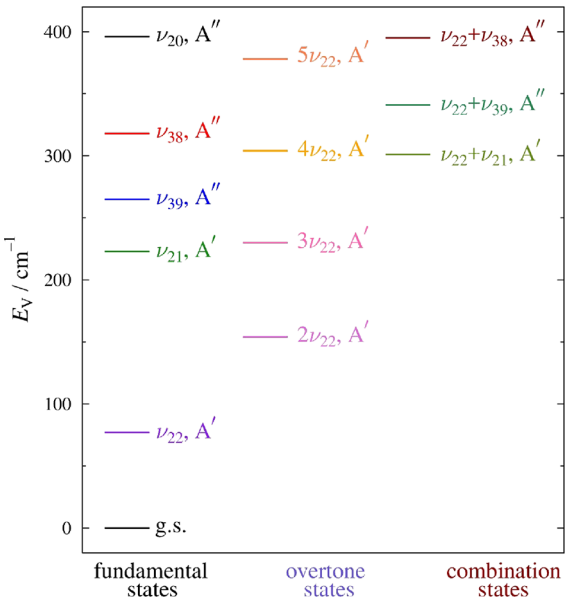

Figure 7. Vibrational energy levels of 1-oxaspiro[2.5]octa-4,7-dien-6-one below 400 cm^{-1}, predicted at the B3LYP/6-311+G(2d,p) level.

the two substituents are moving in opposite directions with respect to the six-membered ring during the vibration. It is perhaps surprising that no perturbations of the transition frequencies were observed due to near-energy ν_{39}, which is expected to be only 30 cm^{-1} higher in energy. These two vibrational states have predicted G_a and G_c values of 320 and 536 MHz, respectively, but appear to be too far apart in energy for the coupling to be observed across the studied frequency range. The $3\nu_{22}$ state is also predicted to be close in energy (A′, 230 cm^{-1} B3LYP, and 205 cm^{-1} MP2). The similar energies of these states are consistent with the transition intensities (*vide infra*) and the total line counts obtained for each data set. It is likely that the allowed *b*-axis coupling constants between these two states are small due to the large change in vibrational quanta between $3\nu_{22}$ and ν_{21}. Additionally, all quartic and sextic centrifugal distortion constants are well determined and are similar to their corresponding ground-state values (Table 2).

Spectral Analysis of $3\nu_{22}$. The spectroscopic constants of the second overtone of ν_{22} ($3\nu_{22}$ A′, 230 cm^{-1} B3LYP; 205 cm^{-1} MP2) are very well predicted from lower-energy members of the v ν_{22} series by linear extrapolation from the lower-quantum states. The transitions were adequately modeled by a sextic distorted-rotor Hamiltonian (Table 2). Due to the lower number of available transitions, H_K, as well as h_1, h_2, and h_3, were held constant at their extrapolated values. From analysis of the v ν_{22} series, it appears that all of the determined spectroscopic constants are physically meaningful (*vide infra*) and free of the effects of untreated couplings.

Spectral Analysis of ν_{39}. The third fundamental, ν_{39} (A″, 265 cm^{-1} B3LYP; 256 cm^{-1} MP2), is a twisting vibration with large motions of the epoxide methylene and the carbon and hydrogen atoms α to the carbonyl group. As shown in Figure 7, this vibrationally excited state is close in energy to $4\nu_{22}$. The close energy of these states increases the likelihood that the transition frequencies of these states are perturbed by Coriolis and anharmonic coupling. Nonetheless, the transitions of ν_{39} could be adequately treated with a single-state, sextic Hamiltonian (σ_{fit} = 42 kHz). Due to the slightly smaller data set of just less than 1700 transitions, h_1 could not be satisfactorily determined, and as a result, its value is held constant at the corresponding ground-state value during the least-squares fitting (Table 2). The remaining spectroscopic constants do not show any of the telltale signs of unaddressed coupling and closely resemble those of the ground and other vibrationally excited states. Without spectroscopic constants from several higher-quantum vibrational states in the ν_{39} series, however, the other sextic centrifugal distortion constants should be viewed with some skepticism. The computed vibration−rotation interaction constants are in the same level of agreement with their experimental values as those for ν_{22} and ν_{21} (Table 3), providing additional support for the spectroscopic constants being free of the impact of coupling. There were no clear gaps in the Loomis−Wood plots or observed resonances for ν_{39}. Due to the spectral density and the many transitions that were visible but excluded from the data set due to underlying spectroscopic features, it is possible that a small number of transition frequencies were influenced slightly by unaddressed coupling.

Spectral Analysis of $4\nu_{22}$. The spectroscopic constants of the third overtone of ν_{22} ($4\nu_{22}$ A′, 304 cm^{-1} B3LYP; 271 cm^{-1} MP2) are very well predicted from lower-energy members of the v ν_{22} series by linear and cubic extrapolation. Due to the spectral density and lower intensity of the transitions of this

Table 3. Experimental and Computed Vibration−Rotation Interaction Constants for Fundamental States of 1-Oxaspiro[2.5]octa-4,7-dien-6-one Analyzed in This Work

	experimental	B3LYP[a]	*obsd − calcd*	MP2[a]	*obsd − calcd*
$A_0 - A_{22}$ (MHz)	14.74163 (15)	14.86	−0.12	15.32	−0.57
$B_0 - B_{22}$ (MHz)	−1.429677 (57)	−1.34	−0.09	−1.43	0.00
$C_0 - C_{22}$ (MHz)	−1.761864 (55)	−1.67	−0.09	−1.78	0.02
$A_0 - A_{21}$ (MHz)	11.25595 (29)	11.64	−0.39	11.55	−0.29
$B_0 - B_{21}$ (MHz)	−1.503753 (84)	−1.45	−0.05	−1.78	0.03
$C_0 - C_{21}$ (MHz)	−1.098401 (77)	−1.05	−0.05	−1.17	0.07
$A_0 - A_{39}$ (MHz)	2.04966 (51)	1.94	0.11	2.25	−0.20
$B_0 - B_{39}$ (MHz)	−0.016908 (98)	0.03	−0.05	−0.09	0.07
$C_0 - C_{39}$ (MHz)	−0.29350 (12)	−0.27	−0.02	−0.32	0.03
$A_0 - A_{38}$ (MHz)	−9.11193 (94)	−9.22	0.11	−9.37	0.26
$B_0 - B_{38}$ (MHz)	0.03368 (17)	−0.01	0.04	0.01	0.02
$C_0 - C_{38}$ (MHz)	0.47281 (20)	0.46	0.01	0.46	0.01

[a]Evaluated with the 6-311+G(2d,p) basis set.

https://doi.org/10.1021/acs.jpca.3c07049
J. Phys. Chem. A 2024, 128, 191−203

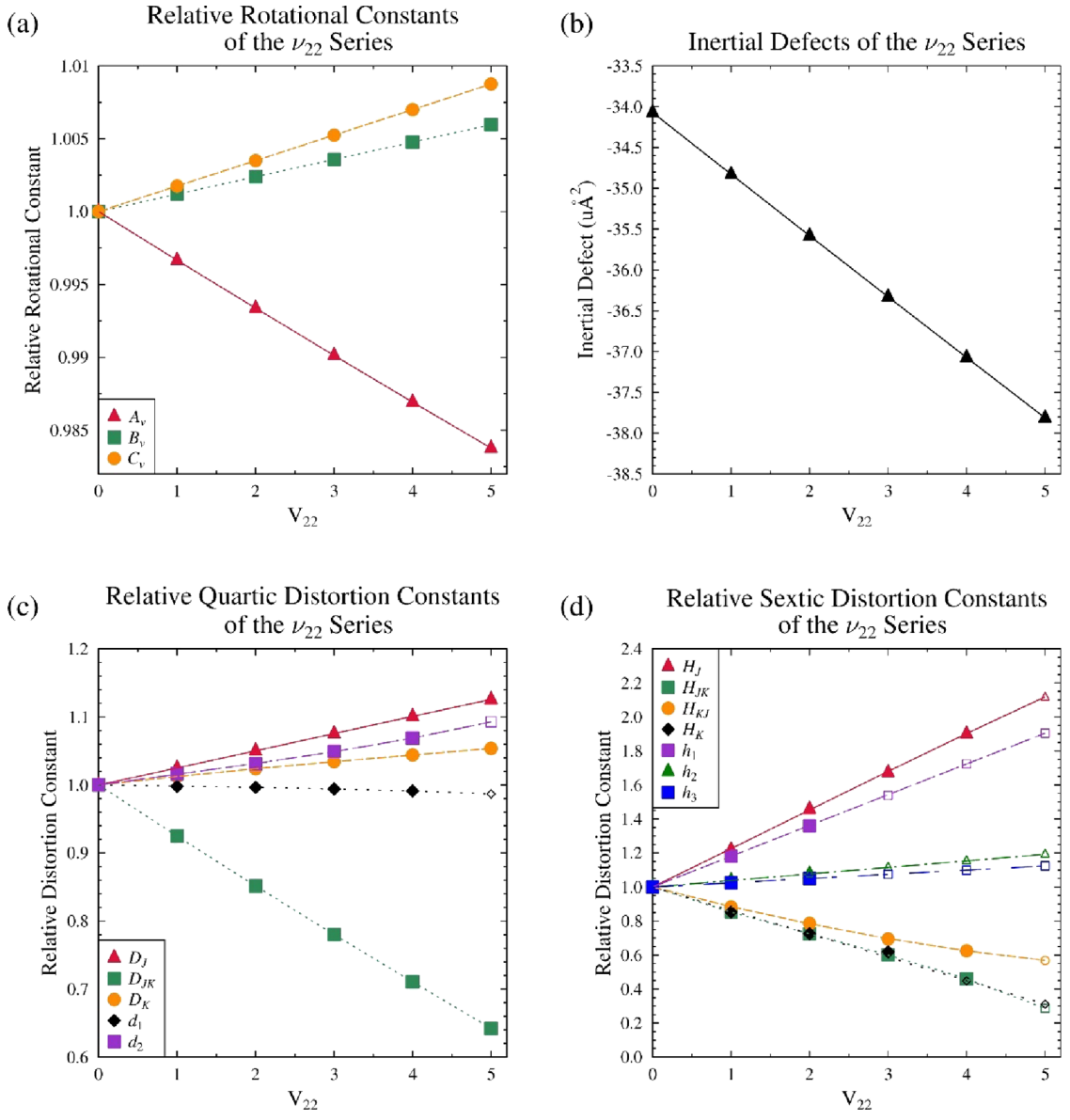

Figure 8. (a) Relative rotational constants, (b) inertial defect, (c) relative quartic centrifugal distortion constants, and (d) relative sextic centrifugal distortion constants for the v ν_{22} vibrational series of 1-oxaspiro[2.5]octa-4,7-dien-6-one as a function of vibrational excitation (v ν_{22} = 0, 1, 2, 3, 4, 5). Open symbols represent points held constant at their extrapolated values in their least-squares fits.

state, only about 1100 transitions were able to be assigned, measured, and included in the least-squares fit (Table 2). Similar to $3\nu_{22}$, the least-squares fit required that H_K, h_1, h_2, and h_3 be held constant at their extrapolated values. There are several other vibrationally excited states in the proximity of $4\nu_{22}$ (ν_{39}, $\nu_{22} + \nu_{21}$, and ν_{28}). Despite the potential for a polyad of states with complex coupling interactions, no obvious perturbation of the transitions was observed.

Spectral Analysis of $\nu_{22} + \nu_{21}$. The lowest-energy combination state, $\nu_{22} + \nu_{21}$ (A′, 301 cm^{-1} B3LYP; 278 cm^{-1} MP2), is very well predicted using linearly extrapolated constants from the ground state (ν_{21}) and ν_{22}. Fewer than 1000 transitions were able to be assigned, measured, and included in the least-squares fit. Despite the lower number of transitions compared with the previously mentioned states, a sextic Hamiltonian model was needed to treat the data set (Table 2). The experimental rotational constants are all within 120 kHz (0.003%) of their extrapolated values, and the quartic centrifugal distortion constants are within 0.73 Hz (1.7%) of their extrapolated values. This close agreement provides independent confirmation of the high-quality nature of the rotational and quartic centrifugal constants of the states used in the extrapolation. In contrast, the sextic centrifugal distortion constants have values that differ significantly from their linearly extrapolated values. Despite the large percentage changes between the observed and extrapolated values, all of the sextic distortion constants that were varied in the least-squares fit have the correct sign and approximate magnitude. Holding these constants to their extrapolated values increased the error of the least-squares fit substantially, so they were allowed to vary in order to obtain a low-error fit. The origin of the disagreement between the observed and extrapolated values may be due to the impact of untreated Coriolis coupling with nearby states. The spectral congestion, however, makes it difficult to determine if the transitions not included in the fit

https://doi.org/10.1021/acs.jpca.3c07049
J. Phys. Chem. A 2024, 128, 191−203

are perturbed or merely obscured by the many observable and likely overlapping transitions.

Spectral Analysis of ν_{38}. The last fundamental observed in this work, ν_{38} (A″, 318 cm^{-1} B3LYP; 310 cm^{-1} MP2), is a lateral wagging motion of the epoxide unit with respect to the six-membered ring. Only about 750 transitions were observed for this vibrationally excited state due in part to its lower intensity. It is also possible that the single-state model may not have been sufficient to model all of the transitions. The sextic constants h_1, h_2, and h_3 could not be satisfactorily determined, and as a result, their values were held constant at the corresponding ground-state value during the least-squares fitting (Table 2). Transitions lacking boosted intensity arising from K_a or K_c degeneracy were difficult to measure, assign, and least-squares fit due to the spectral density. It is possible, however, that the loss of clearly assignable transitions in the Loomis−Wood plots is not just due to a 50% reduction in signal intensity as degeneracy is lost but also due to the impact of Coriolis coupling, which perturbs those transition frequencies. Nonetheless, the agreement between the computed and experimental vibration−rotation interaction constants is excellent, with the largest discrepancy being only 260 kHz (Table 3). A comparison of the quartic and sextic centrifugal distortion constants indicates that these spectroscopic constants are not drastically impacted by the Coriolis coupling. Each value has the same sign and approximately the same magnitude as those of the other fundamental states and the ground state. It is possible that by including only transitions that were well predicted by a single-state model, the constants obtained are likely to be physically meaningful.

Spectral Analysis of $\nu_{22} + \nu_{39}$. The next higher-energy vibrational state is $\nu_{22} + \nu_{39}$ (A″, 342 cm^{-1} B3LYP; 323 cm^{-1} MP2), for which 500 transitions were measured, assigned, and least-squares fit. Both *a*-type and *c*-type, R-branch transitions were included in the least-squares fit, although at a more limited range of J and K_a values than lower-energy vibrational states. Due to the more limited data set, only the rotational and quartic distortion constants could be satisfactorily determined (Table 2). All other spectroscopic constants were held constant at values extrapolated from ν_{22}, ν_{39}, and the ground state. All of the experimental rotational constants were in excellent agreement with their extrapolated values, with the largest discrepancy being only 54 kHz (0.0012%). Likewise, the quartic centrifugal distortion constants were in excellent agreement and differed from their extrapolated values by less than 0.4%. While it is possible that there is a Coriolis interaction with ν_{38} or $5\nu_{22}$, there is no clear evidence of this interaction in the spectral data or spectroscopic constants. As with ν_{38}, the loss of degeneracy in R-branch transitions coincided with an inability to measure a significant number of additional transitions. We cannot preclude that this complication arises due to unaddressed coupling between near-energy states.

Spectral Analysis of $5\nu_{22}$. The final overtone observed for the v ν_{22} series is $5\nu_{22}$ (A″, 378 cm^{-1} B3LYP; 336 cm^{-1} MP2). It is perhaps surprising that a comparable number of transitions could be measured for $5\nu_{22}$ and $\nu_{22} + \nu_{39}$, despite the fact that $5\nu_{22}$ is higher in energy. The data set for $5\nu_{22}$ includes approximately 500 transitions. Only the rotational and on-diagonal quartic centrifugal distortion constants could be varied in the least-squares fit (Table 2). The other spectroscopic constants of the sextic distorted-rotor Hamiltonian employed were held constant at their extrapolated values by using cubic or linear extrapolations as appropriate. The spectroscopic constants that were able to be determined were in excellent agreement with the extrapolated values and help validate the physical meaningfulness of the spectroscopic constants of the lower-quantum states (*vide infra*). It is possible that this state is interacting with the lower-energy states already discussed and the higher-energy states $\nu_{22} + \nu_{38}$ and ν_{20}, which are not reported in the current work.

DISCUSSION

The availability of many quanta of ν_{22} allows a more rigorous analysis of the spectroscopic constants than that available for the other fundamental states in this work. The increase in vibrational quanta should produce a smooth behavior in the spectroscopic constants across the v ν_{22} series, which can be used to validate the spectroscopic constants produced in each of the individual least-squares fits, in particular, to confirm that they have not been significantly contaminated by untreated perturbations. Figure 8 shows the spectroscopic constants through the sextic centrifugal distortion terms across the v ν_{22} series. The rotational constants and inertial defects show remarkable smoothness and remarkable linearity across the series, with R^2 values for a fit to a linear model greater than 0.9999. The experimentally determined quartic centrifugal distortion constants (on-diagonal through $5\nu_{22}$ and off-diagonal through $4\nu_{22}$) show a smooth trend across the series. These series do have a slight curvature that is difficult to discern visually. The off-diagonal constants, d_1 and d_2, were not able to be determined experimentally for higher-quantum members of the series at values that corresponded to the trend of the lower-quantum states (indicated by their open symbols on the plot). This situation arises because of the lower number of available transitions and concomitantly reduced range of K_a quantum number values. As a result, the off-diagonal quartic centrifugal distortion terms were held constant at values extrapolated using an appropriate polynomial, *e.g.*, a cubic model using five data points, v ν_{22}, where v = 0, 1, 2, 3, and 4. Similarly, the experimentally determined sextic centrifugal distortion constants display smooth trends across the series. Where values could not be determined satisfactorily from the experimental data set, they were held constant at values extrapolated from the lower-quantum states using an appropriate polynomial. Using this approach, we are confident that the values used for the centrifugal distortion constants that are held constant have a minimal impact on the physical meaningfulness of the remaining constants. As no readily available software package can currently estimate the quartic or sextic centrifugal distortion constants for the vibrationally excited states, this type of analysis provides the most reliable metric for determining the physical meaning of the ν_{22} spectroscopic constants. As a complete set of spectroscopic constants for a sextic centrifugally distorted-rotor Hamiltonian was determined for ν_{22} and the majority of these constants have been shown to extrapolate very well to higher quanta, ν_{22} serves as a potential benchmark for future computational studies.

The intensities of the transitions of the vibrationally excited states (I_v) are related to their vibrational energy (cm^{-1}) by eq 1, where h is Planck's constant, c is the speed of light, k_B is the Boltzmann constant, and T is the temperature.

$$E_V = -\frac{k_B T}{hc}[\ln(I_v) - \ln(I_0)] \quad (1)$$

https://doi.org/10.1021/acs.jpca.3c07049
J. Phys. Chem. A 2024, 128, 191−203

The intensities of transitions from each of the assigned vibrational modes have been measured by using between 25 and 78 transitions over a 10 GHz frequency range. The details of this analysis are provided in the Supporting Information. The resulting energy values are presented in Table 4, along

Table 4. Experimental and Computed Energies for the Lowest-Energy Vibrationally Excited States of 1-Oxaspiro[2.5]octa-4,7-dien-6-one (in cm^{-1})

mode	experimental[a]	anharmonic frequency (MP2)[b]	anharmonic frequency (B3LYP)[b]
ν_{22}	78.8 (4.3)	69	77
$2\nu_{22}$	157.9 (4.4)	137	154
ν_{21}	213.6 (5.3)	210	223
$3\nu_{22}$	247.5 (6.1)	204	230
ν_{39}	260.5 (6.8)	256	265
$\nu_{22} + \nu_{21}$	296.7 (7.4)	278	301
$4\nu_{22}$	319.7 (7.8)	271	304
ν_{38}	330.7 (7.7)	310	318
$\nu_{22} + \nu_{39}$	334.3 (11.2)	323	342
$5\nu_{22}$	422.2 (16.6)	336	378

[a]Statistical uncertainties are expressed as $1\sigma_{mean}$ (see the Supporting Information). [b]Evaluated with the 6-311+G(2d,p) basis set. Overtones $3\nu_{22}$, $4\nu_{22}$, and $5\nu_{22}$ estimated from the anharmonicity constant.[33]

with their B3LYP/6-311+G(2d,p) and MP2/6-311+G(2d,p) computed values. The computed values of the higher-energy overtone states that are not calculated by the Gaussian routine were determined using eq 2, where ν is the fundamental frequency, v_{22} is the vibrational quantum number, and x_{ii} is the anharmonicity constant, in the manner described by Fuß et al.[33]

$$E_{v_{22}} - E_0 = v_{22}\nu + v_{22}x_{22,22}(v_{22} - 1) \quad (2)$$

The estimated experimental uncertainties are the standard deviation of the mean. The experimental uncertainties increase for the higher-energy vibrational states due in large part to the greater impact of underlying transitions on the intensity of those lower-intensity transitions. The vibrationally excited states with greater than two vibrational quanta ($3\nu_{22}$, $4\nu_{22}$, and $5\nu_{22}$) were estimated using eq 2. The B3LYP frequencies are generally in closer agreement with the experimental values than the MP2 anharmonic values. The B3LYP frequencies of ν_{22}, $2\nu_{22}$, ν_{21}, and ν_{39} are within the 1σ statistical uncertainty of their experimental values.

The observation of several quanta for ν_{22} allows the fundamental frequency and anharmonicity constant to be determined from all observed vibrational quanta of the v ν_{22} series. (A similar analysis was performed for ν_{24} of diketene,[34,35] where transition intensities of v ν_{24}, where v = 0, 1, 2, 3, 4, 5 were experimentally determined.) The experimental energies of the v ν_{22} series (v ν_{22}, where v = 0, 1, 2, 3, 4, 5) from their transition intensities are plotted in Figure 9, along with the computed B3LYP and MP2 anharmonic frequencies. From Table 4 and Figure 9, it is clear that the B3LYP frequencies are in closer agreement with the experimental values than the MP2 values, although both underestimate the vibrational frequency. A weighted least-squares fit of the experimental v ν_{22} series was obtained, where the weights on the experimental energies were set to σ^{-2} (see the Supporting Information for details). The plot of the

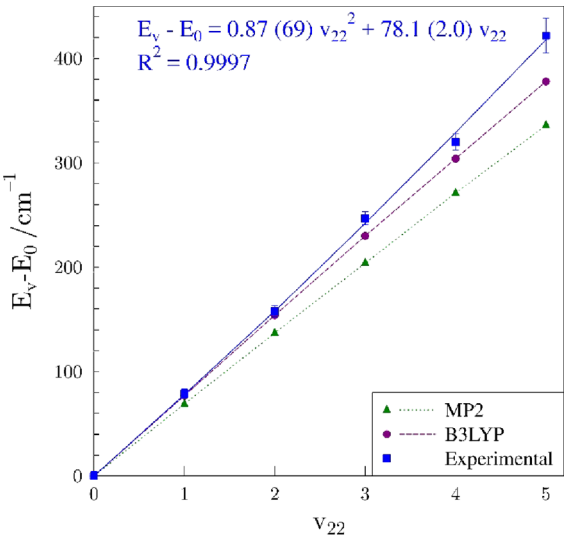

Figure 9. Fundamental frequency (cm^{-1}) of the ν_{22} vibrational mode of 1-oxaspiro[2.5]octa-4,7-dien-6-one derived from measurements of the line intensities of rotational transitions from v ν_{22}, where v = 0, 1, 2, 3, 4, 5.

experimentally determined vibrational energy versus the vibrational quantum number (eq 3; Figure 9) is determined with $R^2 = 0.9997$.

$$E_{v_{22}} - E_0 = [0.87(69)\ cm^{-1}]v_{22}^2 + [78.1(2.0)cm^{-1}]v_{22} \quad (3)$$

The quadratic coefficient is the experimental anharmonicity constant. The fundamental frequency is equal to the linear coefficient plus the anharmonicity constant, while the harmonic frequency is equal to the linear coefficient minus the anharmonicity constant (and a summation of the cross terms with all other vibrational modes, which cannot be addressed in this work).[36] Thus, the fundamental frequency for ν_{22} is experimentally determined to be 79.0 (2.1) cm^{-1} from all observed states of the v ν_{22} series. The fundamental frequency is in excellent agreement with the value determined from a single set of intensity measurements of $1\nu_{22}$ in Table 4 (78.8 (4.3) cm^{-1}), albeit more precisely determined. The larger discrepancy in the MP2 fundamental energy of ν_{22} appears to be due to both an underestimation of the harmonic frequency and an overestimation of the impact of anharmonicity. The computed anharmonicity constants ($x_{22,22}$ = −0.49 and −0.42 cm^{-1}, MP2 and B3LYP, respectively) are of opposite signs and a smaller magnitude than the value determined from the intensity analysis of the v ν_{22} series ($x_{22,22}$ = 0.87 cm^{-1}). The larger uncertainties and thus lower weights of the higher-energy vibrational modes make meaningful determination of the anharmonicity constant difficult. It is possible that the energies of $4\nu_{22}$ and $5\nu_{22}$ are overestimated by eq 1 due to the underlying spectral density, which would cause the value of the experimental anharmonicity constant ($x_{22,22}$ = 0.87 (69) cm^{-1}) to be anomalously large. Because this spectrum is exceptionally dense and the baseline is rarely observed, lower-intensity transitions are systematically increased in intensity due to underlying transitions of other vibrationally excited states. This creates an unfortunate situation wherein the vibrational states that would provide the greatest information regarding the anharmonicity are the ones with the largest statistical

https://doi.org/10.1021/acs.jpca.3c07049
J. Phys. Chem. A 2024, 128, 191−203

uncertainties and are likely to have the largest systematic error in their energies.

CONCLUSIONS

The rotational spectrum of 1-oxaspiro[2.5]octa-4,7-dien-6-one (**1**) was measured for the first time, providing over 5500 transitions between 235 and 360 GHz for the ground vibrational state and thousands more for 10 vibrationally excited states. This frequency range proved to be advantageous as it allowed the measurement, assignment, and least-squares fitting of transitions with J'' ranging from 28 to 179 due to the presence of relatively intense *a*- and *c*-type transitions. Despite the lack of clear band structures in the observed frequency range of this work, the tools available to us (computational predictions and AABS software including Loomis−Wood plots) made analyzing the complex spectrum feasible. Conveniently, the lowest J'' *a*-type transitions and the highest J'' *c*-type transitions observed have shared energy levels, providing redundant information and an excellent determination of the spectroscopic constants. This redundancy will also greatly aid in the extrapolation of transition frequencies outside the observed range for this molecule. At higher frequency, the dominant transitions will be *c*-type transitions whose energy levels are already probed by *a*-type transitions in the current data set. Conversely, at lower frequencies, the dominant transitions will be *a*-type transitions, whose energy levels are likewise probed by *c*-type transitions in the current data set.

The vibrational energies of the lowest-energy fundamental states were indirectly measured via their rotational transition intensities. Due to the inherent difficulties in finding transitions that are free of underlying transitions from other vibrationally excited states, the most reliable of these determinations is undoubtedly the vibrational energy of ν_{22}. The determination of the fundamental energy of ν_{22} from six different quanta (v ν_{22}, where v = 0, 1, 2, 3, 4, 5) makes its energy determination of 79.0 (2.1) cm^{-1} about as accurate and precise as can be expected via this method. A rotationally resolved infrared spectrum should determine the vibrational frequencies very accurately and precisely, although the spectral density may limit the resolution that is achievable. In the absence of a high-resolution infrared spectrum, however, rotational transition intensity analysis of the vibrational states in this work likely provides the most reliable experimental vibrational frequencies.

General Experimental Methods. ^{1}H and $^{13}C\{^{1}H\}$ NMR spectra were recorded using a Bruker Avance III 500 spectrometer at 25 °C (^{1}H 500.1 MHz, ^{13}C 125.7 MHz), and chemical shifts are reported in parts per million (ppm). NMR spectra were referenced to the $SiMe_4$ peak at 0.00 ppm (^{1}H and ^{13}C). High-resolution mass spectra were obtained using a Thermo Q Exactive Plus via ASAP-MS by the mass spectrometry facility at the University of Wisconsin.

*4-(2,2-Dichloroacetoxy)benzyl 2,2-Dichloroacetate (**3**).* This compound was synthesized according to the literature procedure by McLaughlin et al.[3] In a flame-dried round-bottom flask with a magnetic stir bar, 4-hydroxybenzyl alcohol (**2**) (1.00 g, 8.1 mmol, 1 equiv) was dissolved in 20 mL of dichloromethane (dried over 10% m/v 3 Å molecular sieves) with stirring under a nitrogen atmosphere.[37] The solution was then cooled to 0 °C in an ice bath, pyridine (1.30 mL, 16.1 mmol, 2 equiv) was added through a septum, and the resulting solution was stirred for 5 min. Dichloroacetyl chloride (1.71 mL, 17.7 mmol, 2.2 equiv) was then added dropwise to the stirred solution, after which point the reaction mixture was removed from the ice bath and stirred at room temperature, while the reaction was tracked by TLC (30% ethyl acetate in hexanes as the solvent system, with UV visualization). After TLC indicated that 4-(hydroxymethyl)phenol was fully consumed (20 min of stirring at room temperature), the reaction mixture was purified by vacuum filtration through silica gel: 100 g of silica gel was wet-loaded with dichloromethane into a glass-fritted Büchner funnel, and the reaction mixture was loaded onto the silica and then eluted using vacuum with 150 mL of dichloromethane as the eluting solvent. The filtrate was concentrated under reduced pressure, yielding 4-(2,2-dichloroacetoxy)benzyl 2,2-dichloroacetate (**3**) (2.41 g, 7.0 mmol, 86% yield) as a pale-yellow oil. ^{1}H NMR (500 MHz, $CDCl_3$) δ 7.49−7.43 (m, 2H), 7.25−7.18 (m, 2H), 6.16 (s, 1H), 5.98 (s, 1H), 5.29 (s, 2H). $^{13}C\{^{1}H\}$-NMR (126 MHz, $CDCl_3$) δ: 164.27, 162.83, 150.41, 132.95, 129.88, 121.20, 68.07, 64.12, 64.08.

*1-Oxaspiro[2.5]octa-4,7-dien-6-one (**1**).* This compound was synthesized according to the literature procedure by McLaughlin et al.[3] 4-(2,2-Dichloroacetoxy)benzyl 2,2-dichloroacetate (**3**) (2.41 g, 7.0 mmol, 1 equiv) was dissolved with 28 mL of acetonitrile in a round-bottom flask with a magnetic stir bar and cooled to −5 °C in a 1:1 mixture of brine and ice. As the solution was stirred, 30% hydrogen peroxide (2.8 mL, 24.2 mmol, 3.5 equiv) was added to the flask. In a separate flask, a slurry of powdered potassium hydroxide (1.22 g, 24.2 mmol, 3.5 equiv) in 112 mL of acetonitrile was cooled to −5 °C with vigorous stirring. The contents of the first flask were then added to this slurry, and the reaction mixture was stirred at −5 °C for 20 min with TLC tracking (30% ethyl acetate in hexanes as the solvent system with UV visualization). Upon consumption of the starting material, the reaction mixture was partitioned across 200 mL of ethyl acetate and 200 mL of water and the layers were separated. The aqueous layer was then extracted three times with 100 mL of ethyl acetate, and the organic layers were combined and were washed with 100 mL of brine. The combined organic layers were then dried over anhydrous magnesium sulfate and concentrated under reduced pressure. The resulting crude yellow oil was then purified by flash column chromatography (30% ethyl acetate in hexanes), and the pure, product-containing fractions were pooled and concentrated under reduced pressure in a tared vial. This procedure yielded 1-oxaspiro[2.5]octa-4,7-dien-6-one (**1**) (338.6 mg, 2.8 mmol, 40% yield) as an off-white, low-melting solid, which was characterized by ^{1}H and ^{13}C NMR in $CDCl_3$ and by high-resolution ESI-MS. ^{1}H NMR (500 MHz, $CDCl_3$) δ 6.51 (d, J = 2.2 Hz, 4H), 3.35 (s, 2H). $^{13}C\{^{1}H\}$-NMR (126 MHz, $CDCl_3$) δ: 185.36, 146.25, 133.73, 55.07, 53.75. HRMS (ASAP-MS) calculated [M + 1]: 123.0041; observed [M + 1]: 123.0439.

ASSOCIATED CONTENT

Data Availability Statement

The data are available in the manuscript and Supporting Information.

Supporting Information

The Supporting Information is available free of charge at https://pubs.acs.org/doi/10.1021/acs.jpca.3c07049.

Data set distribution plots for vibrationally excited states of 1-oxaspiro[2.5]octa-4,7-dien-6-one (**1**); experimental spectroscopic constants for ground state and vibration-

https://doi.org/10.1021/acs.jpca.3c07049
J. Phys. Chem. A 2024, 128, 191−203

ally excited states of 1-oxaspiro[2.5]octa-4,7-dien-6-one (**1**) in A reduction; analysis of intensities of rotational transitions to provide vibrational energies; details of synthesis and purification; experimental ^{1}H NMR, ^{13}C{^{1}H} NMR, and mass spectra (PDF)

Computational output files, least-squares fitting files for all vibrational states, spreadsheet for intensity/energy analysis, Python script for intensity analysis (ZIP)

AUTHOR INFORMATION

Corresponding Authors

R. Claude Woods − *Department of Chemistry, University of Wisconsin−Madison, Madison, Wisconsin 53706, United States;* orcid.org/0000-0003-0865-4693; Email: rcwoods@wisc.edu

Robert J. McMahon − *Department of Chemistry, University of Wisconsin−Madison, Madison, Wisconsin 53706, United States;* orcid.org/0000-0003-1377-5107; Email: robert.mcmahon@wisc.edu

Authors

Brian J. Esselman − *Department of Chemistry, University of Wisconsin−Madison, Madison, Wisconsin 53706, United States;* orcid.org/0000-0002-9385-8078

Edward B. Pimentel − *Department of Chemistry, University of Wisconsin−Madison, Madison, Wisconsin 53706, United States*

William H. Styers − *Department of Chemistry, University of Wisconsin−Madison, Madison, Wisconsin 53706, United States*

Dairen R. Jean − *Department of Chemistry, University of Wisconsin−Madison, Madison, Wisconsin 53706, United States*

Complete contact information is available at: https://pubs.acs.org/10.1021/acs.jpca.3c07049

Notes

The authors declare no competing financial interest.

ACKNOWLEDGMENTS

We gratefully acknowledge the National Science Foundation for support of this project (CHE-1954270). The Thermo Q Exactive Plus mass spectrometer was funded by NIH Award 1S10 OD020022-1 to the Department of Chemistry, and the Bruker 500 NMR spectrometer was funded by a generous gift from Paul J. and Margaret M. Bender. E.B.P. thanks the William B. Dickinson Annual Fellowship in Organic Chemistry for support. D.R.J. thanks the Department of Chemistry and Life Science, United States Military Academy, for graduate education funding. We thank Maria Zdanovskaia for thoughtful proofreading and suggested edits.

REFERENCES

(1) Schnitzler, E. G.; Jäger, W. The benzoic acid−water complex: A potential atmospheric nucleation precursor studied using microwave spectroscopy and ab initio calculations. *Phys. Chem. Chem. Phys.* **2014**, *16*, 2305−2314.

(2) Onda, M.; Asai, M.; Takise, K.; Kuwae, K.; Hayami, K.; Kuroe, A.; Mori, M.; Miyazaki, H.; Suzuki, N.; Yamaguchi, I. Microwave spectrum of benzoic acid. *J. Mol. Struct.* **1999**, *482*−*483*, 301−303.

(3) McLaughlin, M. F.; Massolo, E.; Cope, T. A.; Johnson, J. S. Phenolic Oxidation Using H_2O_2 via in Situ Generated *para*-Quinone Methides for the Preparation of *para*-Spiroepoxydienones. *Org. Lett.* **2019**, *21*, 6504−6507.

(4) Ohkata, K.; Tamura, Y.; Shetuni, B. B.; Takagi, R.; Miyanaga, W.; Kojima, S.; Paquette, L. A. Stereoselectivity Control by Oxaspiro Rings during Diels−Alder Cycloadditions to Cross-Conjugated Cyclohexadienones: The *Syn* Oxygen Phenomenon. *J. Am. Chem. Soc.* **2004**, *126*, 16783−16792.

(5) Gallucci, J. C.; Tamura, Y.; Paquette, L. A. Preference for the Diels-Alder addition of dienes *syn* to the O atom in cross-conjugated spirocyclic cyclohexadienones. *Acta Crystallogr. Sect. C* **2004**, *60*, o656−o658.

(6) Kubo, M.; Itoh, Y.; Tsuji, M.; Oda, N.; Takeuchi, H.; Itoh, T. Polymerization of 1-Oxaspiro[2.5]octa-4,7-dien-6-ones. *Macromolecules* **1998**, *31*, 3469−3472.

(7) Salamonczyk, G. M.; Oza, V. B.; Sih, C. J. A concise synthesis of thyroxine (T_4) and 3,5,3′-Triiodo-l-thyronine (T_3). *Tetrahedron Lett.* **1997**, *38*, 6965−6968.

(8) Adler, E.; Holmberg, K.; Ryrfors, L. O.; Szabo-Lin, I.; Guthenberg, C.; Mannervik, B. Periodate Oxidation of Phenols. XIV. Oxidation of *p*-Hydroxybenzyl Alcohol with Periodate and bismuthate. *Acta Chem. Scand. B* **1974**, *28*, 883.

(9) Eistert, B.; Bock, G. Reaktionen von α-Dicarbonylverbindungen und Chinonen mit Diazoalkanen, II. Die Umsetzung einiger substituierter *p*-Benzochinone mit Diazomethan zu *p*-Epoxymethyl-cyclohexadienonen. *Chem. Ber.* **1959**, *92*, 1247−1257.

(10) Boulebnane, H.; Roussy, G.; Villamañan, R. M.; Alami, W.; Iratcabal, P. The gas-phase molecular structure of 1-thia-spiro[2.5]-octane: A microwave and molecular mechanics study. *J. Mol. Spectrosc.* **1988**, *132*, 152−157.

(11) Boulebnane, H.; Roussy, G.; Iratcabal, P. Conformational analysis of gaseous 1-oxa-spiro[2.5]octane by microwave spectroscopy and molecular mechanics calculations. *J. Mol. Struct.* **1988**, *190*, 7−15.

(12) Boulebnane, H.; Roussy, G.; Iratçabal, P. 6,6-dimethyl-1-oxa-spiro[2.5]octane. Conformational equilibrium in the gas phase as studied by microwave spectroscopy and molecular mechanics calculations. *J. Mol. Struct.* **1987**, *160*, 259−266.

(13) Harmony, M. D.; Mathur, S.; Choe, J.-I.; Kattija-Ari, M.; Howard, A. E.; Staley, S. W. Complete microwave structure and electron distribution for spiro[2.4]hepta-4, 6-diene. *J. Am. Chem. Soc.* **1981**, *103*, 2961−2966.

(14) Staley, S. W.; Howard, A. E.; Harmony, M. D.; Mathur, S.; Kattija-Ari, M.; Choe, J.-I.; Lind, G. Microwave spectrum, dipole moment, and structure of spiro[2.4]hepta-4, 6-diene. Evidence for significant cyclopropyl conjugation. *J. Am. Chem. Soc.* **1980**, *102*, 3639−3640.

(15) Slafer, W. D.; English, A. D.; Harris, D. O.; Shellhamer, D. F.; Meshishnek, M. J.; Aue, D. H. Microwave spectrum, molecular structure, and dipole moment of oxaspiro[2.2]pentane. *J. Am. Chem. Soc.* **1975**, *97*, 6638−6646.

(16) Weitz, E.; Scheffer, A. Über die Einwirkung von alkalischem Wasserstoffsuperoxyd auf ungesättigte Verbindungen. *Ber. Dtsch. Chem. Ges.* **1921**, *54*, 2327−2344.

(17) Wang, Z. Weitz-Scheffer Epoxidation In *Comprehensive Organic Name Reactions and Reagents*; John Wiley & Sons, 2010; pp 2975−2979.

(18) Amberger, B. K.; Esselman, B. J.; Stanton, J. F.; Woods, R. C.; McMahon, R. J. Precise equilibrium structure determination of hydrazoic acid (HN_3) by millimeter-wave spectroscopy. *J. Chem. Phys.* **2015**, *143*, 104310.

(19) Esselman, B. J.; Amberger, B. K.; Shutter, J. D.; Daane, M. A.; Stanton, J. F.; Woods, R. C.; McMahon, R. J. Rotational Spectroscopy of Pyridazine and its Isotopologs from 235−360 GHz: Equilibrium Structure and Vibrational Satellites. *J. Chem. Phys.* **2013**, *139*, 224304.

(20) Pickett, H. M. Determination of collisional linewidths and shifts by a convolution method. *Appl. Opt.* **1980**, *19*, 2745−2749.

(21) Kisiel, Z.; Pszczółkowski, L.; Medvedev, I. R.; Winnewisser, M.; De Lucia, F. C.; Herbst, E. Rotational Spectrum of *trans*−*trans* Diethyl Ether in the Ground and Three Excited Vibrational States. *J. Mol. Spectrosc.* **2005**, *233*, 231−243.

(22) Kisiel, Z.; Martin-Drumel, M.-A.; Pirali, O. Lowest vibrational states of acrylonitrile from microwave and synchrotron radiation spectra. *J. Mol. Spectrosc.* **2015**, *315*, 83−91.
(23) Pickett, H. M. The fitting and prediction of vibration-rotation spectra with spin interactions. *J. Mol. Spectrosc.* **1991**, *148*, 371−377.
(24) Kisiel, Z., Assignment and Analysis of Complex Rotational Spectra. In *Spectroscopy from Space*, Demaison, J.; Sarka, K.; Cohen, E. A., Eds. Springer Netherlands: Dordrecht, 2001; pp 91−106.
(25) Kisiel, Z. *PROSPE-Programs for ROtational SPEctroscopy*; http://info.ifpan.edu.pl/~kisiel/prospe.htm.
(26) Schmidt, J. R.; Polik, W. F. *WebMO Enterprise, 17.0.012e*; WebMO, LLC.: Holland, MI, USA, 2017; http://www.WebMO.net.
(27) Frisch, M. J.; Trucks, G. W.; Schlegel, H. B.; Scuseria, G. E.; Robb, M. A.; Cheeseman, J. R.; Scalmani, G.; Barone, V.; Petersson, G. A.; Nakatsuji, H., et al. *Gaussian 16 rev C.01*; Gaussian, Inc.: Wallingford, CT, USA, 2016.
(28) Ferres, L.; Mouhib, H.; Stahl, W.; Schwell, M.; Nguyen, H. V. L. Molecular structure and ring tunneling of phenyl formate as observed by microwave spectroscopy and quantum chemistry. *J. Mol. Spectrosc.* **2017**, *337*, 59−64.
(29) Dorosh, O.; Białkowska-Jaworska, E.; Kisiel, Z.; Pszczółkowski, L.; Kańska, M.; Krygowski, T. M.; Mäder, H. The complete molecular geometry and electric dipole moment of salicyl aldehyde from rotational spectroscopy. *J. Mol. Spectrosc.* **2017**, *335*, 3−12.
(30) Caminati, W.; Melandri, S.; Corbelli, G.; Favero, L. B.; Meyer, R. Chair conformation and barrier to ring puckering in 1,3-benzodioxole. *Mol. Phys.* **1993**, *80*, 1297−1315.
(31) Tanaka, K.; Honjo, H.; Tanaka, T.; Kohguchi, H.; Ohshima, Y.; Endo, Y. Determination of the proton tunneling splitting of tropolone in the ground state by microwave spectroscopy. *J. Chem. Phys.* **1999**, *110*, 1969−1978.
(32) Zdanovskaia, M. A.; Franke, P. R.; Esselman, B. J.; Billinghurst, B. E.; Zhao, J.; Stanton, J. F.; Woods, R. C.; McMahon, R. J. Vibrationally excited states of 1*H*- and 2*H*-1,2,3-triazole isotopologues analyzed by millimeter-wave and high-resolution infrared spectroscopy with approximate state-specific quartic distortion constants. *J. Chem. Phys.* **2023**, *158*, 044301.
(33) Fuß, W.; Robertson, E. G.; Medcraft, C.; Appadoo, D. R. T. Vibrational Anharmonicities and Reactivity of Tetrafluoroethylene. *J. Phys. Chem. A* **2014**, *118*, 5391−5399.
(34) Orr, V. L.; Esselman, B. J.; Dorman, P. M.; Amberger, B. K.; Guzei, I. A.; Woods, R. C.; McMahon, R. J. Millimeter-wave Spectroscopy, X-ray Crystal Structure, and Quantum Chemical Studies of Diketene − Resolving Ambiguities Concerning the Structure of the Ketene Dimer. *J. Phys. Chem. A* **2016**, *120*, 7753−7763.
(35) In contrast to the diketene work, the model equation employed for 1-oxaspiro[2.5]octa-4,7-dien-6-one does not assume that the vibrational mode is purely harmonic.
(36) Zdanovskaia, M. A.; Martin-Drumel, M.-A.; Kisiel, Z.; Pirali, O.; Esselman, B. J.; Woods, R. C.; McMahon, R. J. The eight lowest-energy vibrational states of benzonitrile: analysis of Coriolis and Darling-Dennison couplings by millimeter-wave and far-infrared spectroscopy. *J. Mol. Spectrosc.* **2022**, *383*, 111568.
(37) Williams, D. B. G.; Lawton, M. Drying of Organic Solvents: Quantitative Evaluation of the Efficiency of Several Desiccants. *J. Org. Chem.* **2010**, *75*, 8351−8354.

https://doi.org/10.1021/acs.jpca.3c07049
J. Phys. Chem. A 2024, 128, 191−203